

Transverse spatial improvement of a transiently pumped soft-x-ray amplifier

K. Cassou,¹ Ph. Zeitoun,² P. Velarde,³ F. Roy,² F. Ogando,³ M. Fajardo,⁴ G. Faivre,² and D. Ros¹

¹Laboratoire d'Interaction du Rayonnement X avec la Matière, Université Paris Sud XI, Orsay France

²Laboratoire d'Optique Appliquée, ENSTA, Palaiseau, France

³Instituto de Fusión Nuclear, Universidad Politécnica de Madrid, Madrid, Spain

⁴Centro de Física de Plasmas, Instituto Superior Técnico, 1049-001 Lisbon, Portugal

(Received 3 November 2005; published 9 October 2006)

A soft-x-ray laser amplifier based on plasma solid target with a weak transverse refraction and a large gain zone is numerically investigated. A two-dimensional hydrodynamic code ARWEN with radiation transport solved by multigroup method based on adaptive mesh refinement has been used to describe the spatial and temporal plasma evolution. An iron target is transiently pumped creating gain on the $J=0-1$ neonlike transition at $\lambda=25.5$ nm. We show that using a super-Gaussian, instead of Gaussian, transverse spatial laser driver profile leads to a reduction of the transverse refraction by two orders of magnitude and to an enlargement of the gain zone surface by about a factor of 2.

DOI: 10.1103/PhysRevA.74.045802

PACS number(s): 42.55.Vc, 41.75.Jv, 52.59.Ye, 52.65.-y

In recent years, worldwide soft-x-ray laser research has progressed to the point where many laboratories have routinely been able to produce stimulated emission over a wide range of wavelengths. While the search for new and more efficient routes to achieve soft-x-ray lasing continues, there is a steady shift of current research effort to control and hence optimize various properties of soft-x-ray beam. Demonstration of multimillijoule soft-x-ray laser has been achieved in the quasisteady-state (QSS) collisional pumping scheme [1]. Significant progress has also been made in the past few years to push the soft-x-ray lasers toward higher intensity, shorter pulse duration, shorter wavelength, and particularly much higher repetition rate with much less pumping laser energy. These accomplishments were made by the use of high-repetition-rate laser system, and the implementation of the transient-collisional-excitation (TCE) x-ray laser scheme [2,3].

Despite these major improvements, the TCE scheme suffers from a recurrent problem that slows down its opening to new applications. Indeed, the soft-x-ray laser beam generated in the TCE scheme is often poorly homogeneous exhibiting many large- and small-scale structures. Since the beam homogeneity is a key parameter for focusing applications or imaging experiments, such a problem has to be solved. These structures originate from two separate phenomena. First, specklelike pattern is generated from the interferences of several incoherent subpupils [4]. This effect may be easily alleviated by seeding the amplifier with a nearly fully coherent source such as high harmonic generation [5]. This has been achieved recently [6] and opens the route to a new generation of soft-x-ray lasers. The second phenomenon is the beam degradation because of its propagation along the plasma amplifier that is nonhomogeneous. Control and improvement of the plasma homogeneity remains one of the key studies for the increase of soft-x-ray laser performance. More precisely, the nonuniformity of the plasma density induces a spatial fluctuation of the index of refraction that in turn refracts the soft-x-ray laser beam. Note that the larger the density gradients are, the worse the beam quality is. Because of the short pulse pumping, TCE intrinsically generates much larger density gradients than QSS pumping

schemes based on longer pulse duration. Although soft-x-ray laser beam degradation was observed on other pumping schemes, it was not as crucial as now with the transient scheme. Deleterious effects of refraction associated to the transient scheme consist in beam degradation but also in the reduction of the output soft-x-ray laser energy by refracting the beam out of the gain region before reaching the end of the amplifier [7].

All the previous works related to the refraction underwent by soft-x-ray laser have shown that the refraction impacts the beam propagation in not only horizontal but also in vertical directions (Fig. 1). It has been demonstrated that the use of bent target and pre- or double-pulse pumping compensate for horizontal refraction of the soft-x-ray beams in the plasma [8,9]. However, neither bent target nor multipulse pumping alleviate the beam degradation and reduced amplification due to vertical refraction because density gradients along the vertical refraction are much higher than horizontal gradients. The hydrodynamic of soft-x-ray plasma amplifier is a bidi-

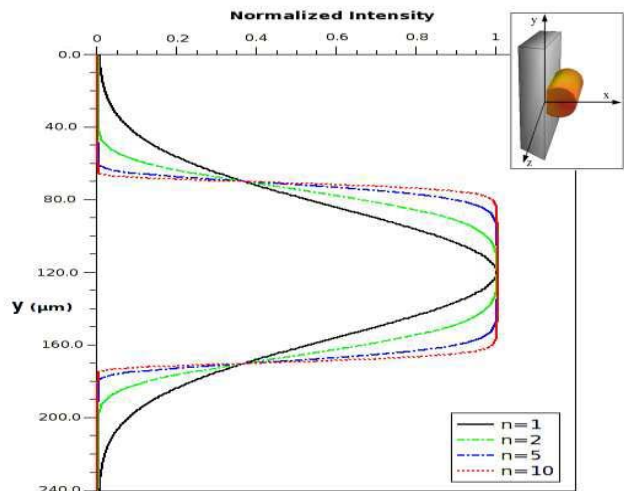


FIG. 1. (Color online) Plot of the laser energy depositions for Gaussian and hyper-Gaussian profiles of different orders. The inset shows the geometry considered.

mensional problem. Up to now, vertical refraction has been treated only with phenomenological modeling using 1.5D hydrocode post-processed by ray-tracing code but assuming *ab initio* plasma vertical profiles [10]. This approach prevents one from a realistic description of plasma structure along the vertical direction. As it will be pointed out in this paper, the two dimensional (2D) effects are strongly impacting the plasma shape, requiring a full 2D hydrocode for approaching a realistic description. Furthermore, the bidimensional modeling pointed out a large overestimation of the vertical size of the gain zone calculated with 1.5D hydrocode.

In this paper we discuss the spatial shaping of the driving laser beam in order to improve the soft-x-ray laser amplifier quality by reducing the vertical refraction combined with a broadening of the amplification surface. We demonstrate by numerical modeling that refraction might be dramatically reduced by using ($n=10$) super-Gaussian laser (SGL) spatial profile instead of the classical Gaussian laser (GL) spatial profile. We also observed that for ($n=10$) super-Gaussian, the gain region size might be increased by a factor of 2 as compared to the Gaussian spatial profile case, doubling the soft-x-ray laser (SXRL) output energy. This additional unexpected result enhances the interest of SGL spatial profile.

A transient collisional SXRL amplifier is typically realized by a combination of a 400 ps pulse (later called “long pulse”) and a 0.7–12 ps pulse both focused on a $0.1 \times 5 \text{ mm}^2$ line, irradiating a solid target. The long pulse creates the plasma. The intensity is chosen such as the maximum plasma ionization stage corresponds to the neonlike ion aiming to produce a large pool of lasing ions. The second intense and short infrared laser pulse instantaneously heats up the plasma free electrons in the high electron density region. These hot electrons collisionally pumps the lasing ions producing transient gain that reaches a value as high as a few 100 cm^{-1} . This peak gain lasts only few picoseconds while the ionization balance stays unchanged in the neonlike stage, until the plasma is overionized mainly by electron-ion collision. Since the ionization balance does not change during the peak gain period, we may realistically consider that the electron density gradients do not evolve from the end of the plasma ionization period until the amplification period. Ponderomotive force which may modify the shape of the density gradient is assumed here to be negligible. Consequently, we may consider that only the long laser pulse shapes the electron density profile sampled by the SXRL beam. These assumptions also consider that the plasma does not evolve significantly during the propagation of the soft-x-ray beam along the amplifier, as is the case for traveling wave pumping. The SGL spatial profile can be realized experimentally by using diffractive optics or by coupling a standard combination of a cylindrical and spherical lens to an adaptive mirror [11]. With this scheme the line focus is achieved thanks to the use of the lenses while the adaptive optic [12] serves to shape the transverse (vertical) profile of the line focus. The longitudinal line shape is normally sufficiently homogeneous to prevent any correction. Here we consider that both the long and short pulses are focused with the same optics meaning that the gain region properties of interest (ions density,

electron density gradient, sizes) are given by the energy deposition of the long pulse while electronic temperature profile is given by the short laser pulse. To model the laser deposition influence and the following hydrodynamic plasma evolution we used the bidimensional (2D) hydrocode ARWEN. The ARWEN [13] code is based on adaptive mesh refinement (AMR) fluid dynamic and radiation transport calculations. The radiation intensity is calculated with a discrete energy multigroup scheme [14] coupled to the adaptive algorithm. To our knowledge this is the first time that an AMR code is used to model SXRL plasmas. As compared to older 2D hydrocodes, AMR technique is much faster enabling to run a full, highly resolved hydrodynamic case in a reasonable CPU time (8 h) as required to achieve a complete case. Simulation are realized with a base cell grid of 128×128 cells and two refinement levels. The radiation transport is initialized with 16 angles. The simulation window is defined by a $240 \mu\text{m}$ square side with a slab target of $10 \mu\text{m}$. The vacuum in front of the target is set at a baking pressure of 10^{-3} mbar.

The goal of hydrodynamic modeling of the laser-produced plasma is to find optimum laser drive spatial conditions for the long laser pulse to obtain the largest possible gain region associated with negligible vertical density gradients (Fig. 1). For the sake of clarity we define the axis along which the soft-x-ray laser propagates as z , the vertical direction y as the axis perpendicular to the driving laser incidence, x direction. For all the simulations of interest, the target is illuminated by a $\lambda=800 \text{ nm}$ laser having a Gaussian pulse duration of 400 ps [full width at half maximum (FWHM)] and 1 J energy corresponding to the typically uncompressed chirped pulse of Ti:Sa laser system. 100 ps after the peak of the long pulse, a second short 5 ps (FWHM) duration pulse of 2 J heats the preformed plasma with temporal and spatial shape identical to the long laser pulse. The spatial deposition profile of the laser pulse energy on the target, modeled by $I = I_0 \exp[-y^2/(2\sigma^2)]^n$, is Gaussian for $n=1$ or super-Gaussian for n greater than 1. Our study has been performed considering the cases of $n=2, 5$, and 10 while we show only the results of the most interesting cases $n=1$ and $n=10$. For all Gaussian or super-Gaussian lasers, the widths at half maximum are set at $100 \mu\text{m}$ (Fig. 1). The target length is set at 5 mm. We assume a homogeneous deposition along the z direction.

Figures 2 and 3 displayed 2D maps of the electron densities and temperatures for $n=1$ (Fig. 2) and $n=10$ (Fig. 3) for early time of laser-matter interaction (200 ps prior to the peak of the long pulse) and for the latter instant at 100 ps after the peak of the long laser pulse when the short pulse heats the plasma. During the early times of the laser-target interaction, the laser pulse shapes strongly imprint Gaussian [Fig. 2(a)] or super-Gaussian [Fig. 3(a)] density profiles. However, later during the plasma evolution, when the short pulse heats up the plasma, the density and temperature profiles do not reproduce so precisely the laser shapes [Figs. 2(b) and 3(b)]. On both plasmas created by Gaussian and super-Gaussian lasers the edges look perturbed. For $n=10$ SGL, at 100 ps after the peak of the pulse, plasma jets appear clearly around $y=40 \mu\text{m}$ and $190 \mu\text{m}$ while the central part of the plasma is homogeneous in terms of electron

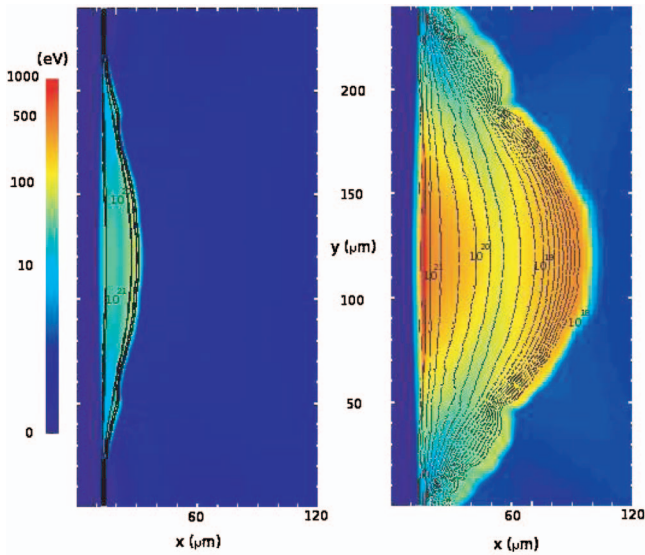


FIG. 2. (Color) 2D plot of temperature in false colors with a logarithmic scale and isodensity contour of electron density in cm^{-3} in logarithmic scale for Gaussian profile ($n=1$). (a) 20 ps before and (b) 100 ps after the peak of the laser pulse.

density and temperature. For both GL and SGL generated plasmas cases, the plasma centers are expanding with the highest velocities because most of the laser energy is laid down there, while the sides are cooler and less dense leading to lower lateral velocities. This results in the plasma inhomogeneities observed on the edges. For plasma created by SGL profile [Fig. 3(a)] there is a weak lateral expansion at the beginning reducing the plasma cooling as compared with plasmas created by GL profile pulse. This is even reinforced by the reduced lateral conduction for the case of plasmas created by super-Gaussian beam. Thus at high electron density ($N_e \approx 10^{20} - 10^{21} \text{ cm}^{-3}$), where the second pulse is absorbed, the GL generated plasma has a temperature of about $T_e \sim 562 \text{ eV}$ at its center $y=120 \mu\text{m}$ dropping to $T_e \sim 200 \text{ eV}$ at $y=75 \mu\text{m}$ and $y=175 \mu\text{m}$. For $n=10$, SGL profile pulse, the peak temperature is nearly the same, however

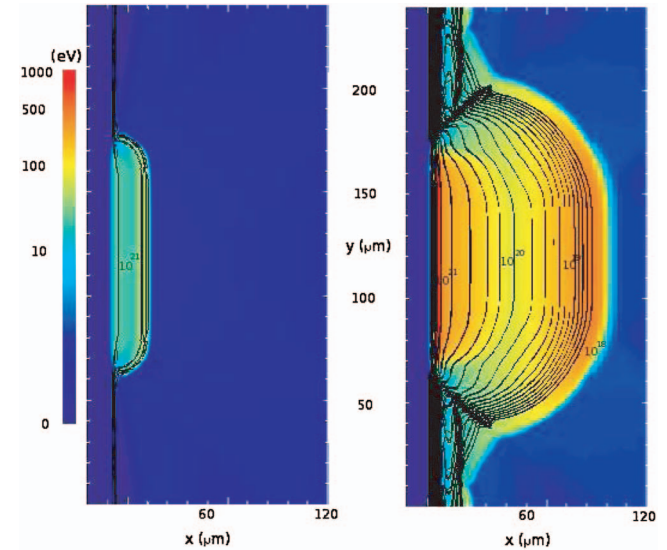


FIG. 3. (Color) 2D plot of temperature in false color with the logarithmic scale and isodensity contours of electron density in cm^{-3} in logarithmic scale for flat-top profile ($n=10$). (a) 200 ps before and (b) 100 ps after the peak of laser pulse.

on the edges ($y=75 \mu\text{m}$ and $y=175 \mu\text{m}$) a much higher temperature of $T_e \sim 320 \text{ eV}$ is achieved. Besides, the density profiles follow somehow the laser deposition profile, creating a kind of plateau on the electron density with sizes increasing with n . For $n=1$, the plateau is about 25% of the laser full width while it rises up to 40% for $n=5$ and up to 60% for $n=10$ SGL profile. The direct consequence of this enlargement of the hottest and densest parts of the plasma, is that neonlike ions, i.e., lasing ions, are found in regions with boundaries at $\pm 25 \mu\text{m}$ from the plasma center for GL pulse, increasing to $\pm 40 \mu\text{m}$ for $n=5$ SGL pulse up to $\pm 50 \mu\text{m}$ for $n=10$. Note that for all GL or SGL cases, lasing ions are found from $x=20 \rightarrow 40 \mu\text{m}$. This means that the potentially amplifying surface, and then the maximum output energy of the SXRL, is multiplied by a factor of 2 for $n=10$ SGL vertical profile as compared to GL. As previously discussed, the electron density gradients, particularly along the y direc-

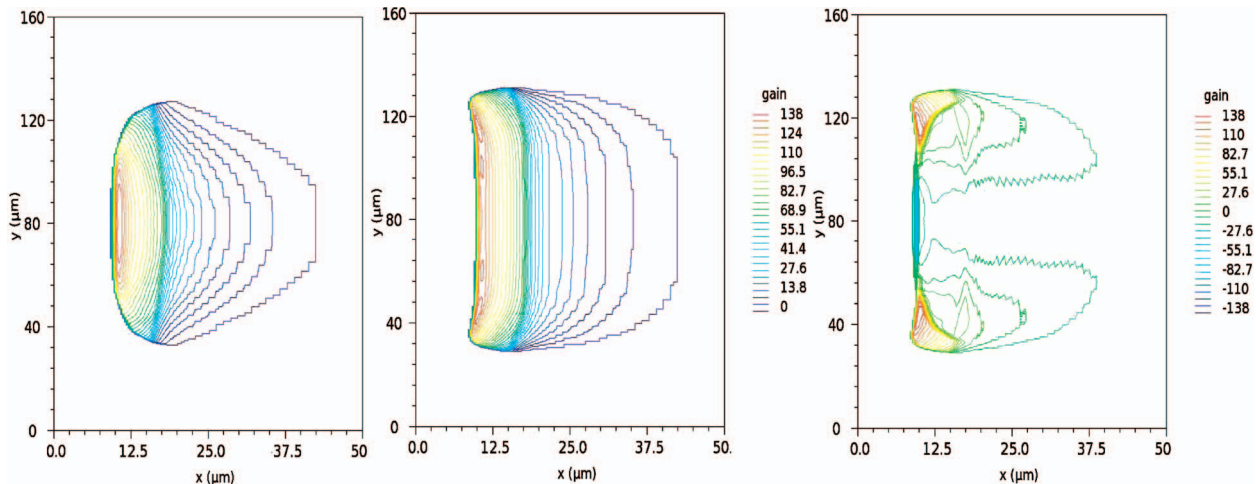


FIG. 4. (Color) Contour maps for the soft-x-ray laser gain at 25.5 nm for different laser drive vertical spatial profiles: (a) Gaussian, (b) super-Gaussian and (c) difference ($b-a'$).

tion, may dramatically reduce the net SXRL amplification and destroy the beam homogeneity. Comparison of figures [Fig. 2(b) and Fig. 3(b)] shows an impressive reduction by more than three orders of magnitude of the vertical density gradient in the region of peak gain localization for $n=10$ SGL ($\nabla_y N_e \approx 1.1 \times 10^{21} \text{ cm}^{-4}$) as compared to $n=1$ case ($\nabla_y N_e \approx 6.0 \times 10^{24} \text{ cm}^{-4}$). Following the calculation in the paraxial approximation propagation of soft-x-ray beam, this shows that the refraction is negligible for ($n=10$) SGL profile [15]. Note that electron density gradients along the x direction are equivalent for any GL- or SGL-produced plasmas ($n=2, 5, 10$).

To achieve 2D gain maps, we postprocessed the outputs of ARWEN with a simplified three-level atomic model. Such a calculation is known to slightly overestimate the gain [16]. We assumed that the fundamental level $1s^2 2s^2 2p^6$ is much more populated than the other levels. The upper lasing level ($1s^2 2s^2 3p J=0$) is linked to the fundamental level by a forbidden transition and following the conclusions of Goldstein *et al.* [17], we assume that is mainly populated by direct collisional excitations. The lower lasing level ($1s^2 2s^2 3s J=0$) is populated and depopulated through both collisional and radiative transitions. Collisional and radiative rates have been obtained from previous works on neonlike iron [18]. Spectral width is calculated assuming both homogeneous and inhomogeneous broadening based on ARWEN output. The electron density is given by ARWEN at the instant of firing the second pulse. From Figs. 4(a) and 4(b) we can observe in the

2D gain maps that the shapes of the gain regions follow the energy deposition profiles.

Close maximum gain, around 136 cm^{-1} , is found for all profiles. Yet, it is interesting to note that the peak gain zone is two times larger over the y direction for the $n=10$ SGL ($80 \mu\text{m}$) as compared to GL case ($40 \mu\text{m}$). To highlight the increase in gain surface for the SGL profile, we displayed the subtraction of the two gain maps in Fig. 4(c), showing two large amplifying areas on the border with gain value around 30 cm^{-1} . We note also that for $x=10 \mu\text{m}$, negative differential gain around -136 cm^{-1} appears, meaning that the gain zone is moved forward a few microns in the Gaussian case.

This study underlines the need of complete bidimensional hydrodynamic code to achieve realistic soft-x-ray plasma amplifier description. Indeed, we show that lateral thermal conduction reduces the gain zone to a third of laser width when Gaussian laser shape is considered. By using a 2D hydrocode, we have numerically demonstrated that $n=10$ SGL spatial profile reduces the vertical refraction to an insignificant level. Consequently, an amplified soft-x-ray beam of high homogeneity would be achievable. Another beneficial phenomenon observed is an enlargement of the gain region surface by a factor of 2 while using super-Gaussian spatial profile as compared to classical Gaussian laser profile. Broadening of effective amplification surface would lead to doubling of the output energy. These two points allow a better output soft-x-ray laser energy extraction ensuring to double the output energy without increasing the driving laser energy.

-
- [1] B. Rus *et al.*, Phys. Rev. A **66**, 063806 (2002).
 - [2] P. V. Nickles *et al.*, Phys. Rev. Lett. **78**, 2748 (1997).
 - [3] J. Dunn *et al.*, Phys. Rev. Lett. **84**, 4834 (2000).
 - [4] O. Guilbaud *et al.*, Europhys. Lett. (to be published).
 - [5] R. Bartels, Nature (London) **406**, 164 (2000).
 - [6] Ph. Zeitoun *et al.*, Nature (London) **431**, 427 (2004).
 - [7] S. Le Pape and Ph. Zeitoun, Opt. Commun. **219**, 323 (2003).
 - [8] J. G. Lunney, Appl. Phys. Lett. **48**, 891 (1986).
 - [9] R. Kodama *et al.*, Phys. Rev. Lett. **73**, 3215 (1994).
 - [10] J. A. Plowes, Opt. Commun. **116**, 260 (1995).
 - [11] G.-Y. Yoon *et al.*, Appl. Opt. **36**, 847 (1997).
 - [12] T. A. Planchon *et al.*, Opt. Commun. **216**, 25 (2003).
 - [13] F. Ogando and P. Velarde, J. Quant. Spectrosc. Radiat. Transf. **71**, 541 (2001).
 - [14] L. H. Howell *et al.*, Numer. Heat Transfer, Part B **35**, 47 (1999).
 - [15] E. Fill, J. Opt. Soc. Am. B **14**, 1505 (1997).
 - [16] Y. Li, G. P. Preztler *et al.*, Phys. Plasmas **4**, 164 (1997).
 - [17] W. H. Goldstein *et al.*, Phys. Rev. A **36**, 3607 (1987).
 - [18] M. Cornille *et al.*, At. Data Nucl. Data Tables **58**, 1 (1994).